Deep-Sea Research II

Characterisation of mesoscale features and phytoplankton variability in the Mozambique Channel.

T. Lamont[a,*], R.G. Barlow[b,c], T. Morris[b], M.A. van den Berg[a]

[a] Oceans & Coasts Research, Department of Environmental Affairs, Private Bag X2, Roggebaai, 8012, South Africa
[b] Bayworld Centre for Research & Education, P.O. Box 7296, Roggebaai, 8012, South Africa
[c] Marine Research Institute, University of Cape Town, Private Bag, Rondebosch, 7701, South Africa
* Corresponding author email: tarron.lamont@gmail.com

Abstract

The variability of hydrographic characteristics and phytoplankton distribution associated with mesoscale eddies in the Mozambique Channel was investigated during four cruises in September 2007, December 2008, November 2009, and April/May 2010. Satellite altimetry was used to map the location of mesoscale features, and together with ETOPO1 bathymetry, it was entered into a Discriminant Function Analysis to classify sampling stations into five categories, namely cyclonic, anti-cyclonic, frontal, divergence, and shelf. Fluorescence profiles were integrated through four depth ranges in the upper 200m and used to determine the depth of the maximum chlorophyll *a* concentration and to model the euphotic zone depth. At a depth of 100 m, distinctly different hydrographic characteristics were observed between mesoscale features, with cyclonic eddies consisting of Subtropical Surface Water, and anti-cyclonic eddies containing Tropical Surface Water from the Indian Ocean. Hydrographic properties at divergence and frontal stations reflected a mixture of these water masses, while shelf stations showed considerable variability determined by the interaction of mesoscale eddies with the continental slope. Chlorophyll *a* concentrations in the surface layers were low, while subsurface levels were significantly greater. Phytoplankton biomass in cyclonic and anti-cyclonic eddies were relatively low and not significantly different. Considerably greater phytoplankton levels were observed in frontal and shelf regions due to the interaction of mesoscale eddies with the continental slope on the western side of the Channel.

Keywords: Mesoscale eddies, Altimetry, Mozambique Channel, Phytoplankton biomass

1. Introduction

The net southward flow through the Mozambique Channel is dominated by poleward-travelling anti-cyclonic eddies which extend to the ocean floor and have diameters typically ranging between

300-350 km (Biastoch and Krauss, 1999; de Ruijter et al., 2002; Ridderinkhof and de Ruijter, 2003). These eddies tend to be formed north of the narrows, near 15 °S, with a frequency of 7 per year which decreases to 4 per year toward the southern end of the Channel due to dissipation or merging of eddies (Backeberg et al., 2008; Schouten et al., 2003). It has been suggested that eddy formation shows a seasonal cycle in relation to the variability in the South Equatorial Current north of Madagascar (Backeberg and Reason, 2010). Southward propagation of the eddies through the Channel occurs at rates of 3-6 $km.d^{-1}$ and they have been shown to interact with the Agulhas Current system further south by initiating the formation of Natal Pulses and by causing a more eastward occlusion of the Agulhas Retroflection, which may lead to the shedding of Agulhas rings into the South Atlantic Ocean (Schouten et al. 2002; van Leeuwen et al., 2000).

In the upper layers, these eddies are known to consist of warm, saline Tropical and Subtropical Surface Water and Indian Central Water (de Ruijter et al., 2002). Intermediate water in the core of the eddies shows meridional variation, with fresher Antarctic Intermediate Water (AAIW) being prominent in the south and more saline Red Sea Intermediate Water (RSIW) observable to the north (Swart et al., 2010). Large heat, salt and nutrient anomalies have been associated with these eddies and it has been demonstrated that they effectively transport these anomalous water properties into the Agulhas Current system as far downstream as Agulhas Rings, thereby contributing to the heat, salt and nutrient fluxes in the South Atlantic Ocean (Roman and Lutjeharms, 2007, 2009; Swart et al., 2010).

Float trajectories suggest considerable mixing between eddies and surrounding waters in the Channel (Chapman et al., 2003), and as these eddies follow a well-defined path along the Mozambican shelf, chlorophyll-enriched coastal water is entrained and transported to the middle of the Channel (Quartly and Srokosz, 2004). As anti-cyclonic eddies interact with the shelf, they are believed to generate cyclonic, lee eddies at prominent coastal offsets, such as off Angoche at about 16 °S (Ridderinkhof and de Ruijter, 2003; Lutjeharms, 2006). These lee eddies result in the upwelling of nutrient-rich water and subsequent increases in phytoplankton biomass. Typically, anti-cyclonic eddies are nutrient-depleted and have low rates of primary production, but it has been noted that these eddies can support production at their edges as a result of high turbulence and isopycnal mixing (Falkowski et al., 1991; Swart et al., 2010). The frontal zones at the edges of eddies have been identified as preferred foraging areas for top predators such as Great Frigate birds, while tuna appear to feed both in the cores and at the frontal zones of the eddies (Weimerskirch et al., 2004; Tew Kai and Marsac, 2010).

Phytoplankton variability in the northern (10°S - 16°S) and southern (24°S - 30°S) parts of the Channel is dominated by the seasonal cycle, with the onset of the bloom marked by a small increase in satellite chlorophyll *a* from December to March, reaching a peak in July-August (Lévy et al., 2007; Tew Kai and Marsac, 2009). Schouten et al. (2005) have demonstrated that intrusions of the South Equatorial Current into the Mozambique Channel show a seasonal cycle, transporting higher chlorophyll *a* Tropical Surface Water during winter and low chlorophyll *a* Subtropical Surface Water in summer. These water masses are characterised by different biogeochemical activity and appear to enhance the amplitude of the seasonal variation of chlorophyll *a* in the Mozambique Channel (Omta et al., 2009). In the central part (16°S - 24°S) mesoscale dynamics drives phytoplankton variability, with anti-cyclonic eddies being associated with low satellite chlorophyll *a* concentrations, while cyclonic eddies were correlated with elevated chlorophyll *a* (Tew Kai and Marsac, 2009).

Knowledge of the influence of mesoscale eddies on ecosystem functioning in the Channel is limited, however, and thus a regional research programme (MESOBIO) was initiated to investigate interactions between the various trophic levels in more detail. Several multi-disciplinary research cruises were staged and physical, chemical, and biological sampling was conducted within mesoscale eddies and frontal regions (Ternon et al., 2012). Phytoplankton species have been described by Bornman et al. (2012), while Barlow et al. (2012) examined the adaptation of phytoplankton populations at the surface and deep chlorophyll maximum (DCM). The objective of this study was to characterise mesoscale features in the Channel and describe the variability of phytoplankton abundance and distribution in relation to these features. The main scientific questions addressed were: (1) Can satellite altimetry be used to classify cyclonic and anti-cyclonic eddies in the Mozambique Channel? (2) Are there significant differences in hydrographic parameters between these features? (3) What is the distribution pattern of phytoplankton biomass within and between these eddies and frontal zones?

2. Data and Methods

2.1. Study region and hydrographic sampling

Hydrographic surveys of mesoscale features in the Mozambique Channel were conducted during September 2007 (cruise MC07, *FRS Algoa*), December 2008 (cruise MC08A, *RV Dr. Fridtjof*

Nansen), November 2009 (cruise MC09B, *RV Antea*), and in April 2010 (cruise MC10A, *RV Antea*) (Fig. 1). At most stations, except those on the shelf, conductivity-temperature-depth (CTD) casts were conducted from the surface to a depth of 1000 m, measuring temperature, salinity, and fluorescence. Discrete water samples were collected at various depths throughout the upper 1000 m for the determination of dissolved inorganic macronutrient and chlorophyll *a* (chla) concentrations. Chlorophyll *a* samples were frozen on board and analysed later according to the fluorometric technique of Welschmeyer (1994). Nutrient samples were either frozen (cruises MC07 and MC08A) or pasteurized (cruises MC09B and MC10A) on board and later analysed by standard auto-analyser techniques (Mostert, 1983; Oudot et al., 1998). The upper limit of the nitracline was defined as the depth (m) at which the change in nitrogen (NO_3 + NO_2) concentration over a 10 m depth interval was ≥ 0.2 µM, as linearly interpolated between discrete sampling depths.

Vertical fluorescence profiles were converted to chlorophyll-equivalents (mg m^{-3}) by calibration with discrete chla concentrations for cruises MC07 and MC08A only. Unfortunately, the fluorescence profile data for cruises MC09B and MC10A were found to be unreliable and could not be used. Examination of the structure of the vertical chla profiles (MC07, MC08A) revealed that most of the phytoplankton biomass was distributed within the upper 200 m. Exceptions to this were found for a few profiles conducted within anticyclonic eddies, but the proportion of biomass below 200 m was insignificant compared to that in the water column above. The structure of the vertical profiles showed consistent patterns for four layers within the upper 200 m. Integrated chlorophyll *a* was therefore computed for each of these layers, namely 0-20 m, 21-100 m, 101-150 m, 151-200 m. For each profile, the depth of the deep chlorophyll maximum (z_{DCM}) was determined as the depth at which the chla reached a maximum value. The depth of the euphotic zone (z_{eu}) was defined as the depth at which the photosynthetically available radiation (PAR) has decreased to 1 % of the value at the surface (Kirk, 1994). z_{eu} is usually derived from the logarithmic interpolation of the vertical PAR profile. PAR data was not available for these cruises and thus the relationship between z_{eu} and the total pigment content within the euphotic zone was used to predict z_{eu} from the vertical chlorophyll *a* profiles, according to Morel and Berthon (1989). This relationship was approximated by two successive linear segments, using the modified coefficients of Morel and Maritorena (2001), and z_{eu} was derived for each vertical profile.

2.2. Satellite altimetry and Discriminant Function Analysis

Weekly averaged maps of delayed-time merged sea surface height anomaly (SSHA) and absolute dynamic topography (ADT) were used to spatially describe and quantify the station locations in relation to mesoscale features observed during the four cruises. The satellite altimetry products were produced by Ssalto/Duacs and distributed by AVISO with support from CNES (http://www.aviso.oceanobs.com/). SSHA and geostrophic current speed (GC) at each station occupied during the surveys were extracted from altimetry maps approximately concurrent with the survey periods, and used together with ETOPO1 bathymetry in a Discriminant Function Analysis (DFA) to statistically group the stations. Due to the difference in temporal resolution between the satellite and in situ data, the same satellite data point was at times used for some of the CTD stations, even though sampling at these stations was conducted several days apart. However, it is believed that this did not significantly bias the classification, since the satellite altimetry represents a period of one week, and the temporal resolution of the CTD sampling did not exceed the translation speed of the mesoscale features.

Five categories, namely Cyclonic (C), Anti-cyclonic (A), Frontal (F), Divergence (D), and Shelf (S) areas, were distinguished in the DFA. The F statistic is a ratio of among-group to within-group variance and was used to determine the extent to which the three variables made unique contributions to the prediction of the various categories. Tolerance estimates, ranging from zero to one, with a threshold of 0.01, were used to evaluate collinearity among the variables used in the DFA. When the tolerance is close to zero, the variance associated with a variable is already accounted for by another, and thus it will not provide significant discrimination in the model (McGarigal et al., 2000). The Wilks' Lambda statistic was used to describe the statistical significance of the DFA, while the partial Wilks' Lambda indicated the discriminatory power of each variable. Both these statistics range from zero to one, indicating greater discriminatory power the closer they are to zero (McGarigal et al., 2000). Standardised canonical coefficients were used to represent the loadings of each variable in the discriminant functions (DFs).

3. Results and Discussion

3.1. Eddy structure and station classification

Satellite altimetry is commonly used to identify and track mesoscale eddies (Chelton et al., 2007; Fu et al., 2010). In the southern hemisphere, anti-cyclonic eddies are identified as anti-clockwise rotations with positive SSHA, while clockwise rotations with negative SSHA indicate cyclonic

eddies (Tew Kai and Marsac 2009; Backeberg et al., 2008). Mature cyclone/anti-cyclone pairs were surveyed in the central part of the Mozambique Channel during cruise MC07 (Fig. 2a), and in the southern part of the Channel during cruise MC09A (Fig. 4a-c). SSHA of 30 cm and 35-40 cm were associated with these cyclonic and anti-cyclonic eddies, respectively. GC varied from about 10 cm s^{-1} in the centres of the eddies to 114 cm s^{-1} in the frontal regions between the eddies. A total of 34 and 54 hydrographic stations were occupied during MC07 and MC09A, respectively.

Several eddies were sampled throughout the Channel during cruises MC08A (Fig. 3a-c) and MC10A (Fig. 5a-d). Anti-cyclonic eddies and frontal regions sampled during these cruises showed SSHA and GC similar in magnitude to those observed during MC07 and MC09A. However, cyclonic eddies observed throughout the Channel during MC08A and in the southern part during MC10A had much weaker SSHA, suggesting that these eddies were either less mature, merging with other eddies, or dissipating. The weakening of SSHA has previously been associated with the dissipation and merging of eddies in the Mozambique Channel (Schouten et al., 2003). A total of 96 and 57 hydrographic stations were sampled during MC08A and MC10A, respectively.

A DFA was used to statistically group the stations into five categories to aid in the description of the mesoscale features. Overall, the discrimination between the five categories was found to be highly significant (Wilks' Lambda = 0.271, F = 17.406, $p < 0.001$). The independent contributions of each variable to the prediction of the discriminant functions (DFs) in the model are shown in Table 1. Partial Wilks' Lambda statistics indicated that SSHA and GC contributed the most to the overall discrimination between the station categories, while the bathymetry contributed the least. Three DFs with respective Chi-squareds of $X^2 = 104.66$, $X^2 = 60.00$, and $X^2 = 21.77$, were identified as statistically significant ($p < 0.001$). DF1 had an eigenvalue of 3.66 and accounted for 48.72 % of the observed variance. DF2 and DF3 had eigenvalues of 2.74 and 1.12, and discriminant capacities of 36.41 % and 14.87 %, respectively. Standardised coefficients (Table 1) indicated that both DF1 and DF2 were most heavily weighted by the SSHA and GC, with the SSHA loading higher on DF1 and the GC loading higher on DF2. DF3 was marked mostly by the bathymetry.

The group centroids and 95 % confidence ellipses for each category (Fig. 6a) indicated that DF1 discriminated primarily between cyclonic, divergence, and anti-cyclonic stations. Cyclonic stations were associated with large negative SSHA (-21.82 ± 7.23 cm) and slower GC (29.96 ± 14.01 cm s^{-1}), while anti-cyclonic stations had large positive SSHA (31.67 ± 7.50 cm) and slightly faster GC (36.84 ± 16.98 cm s^{-1}). Divergence stations typically had small SSHA (-1.38 ± 10.60 cm) and slow

GC (25.70 ± 12.21 cm s^{-1}). DF2 distinguished frontal stations, while DF3 separated shelf stations from the rest (Fig. 6b). Frontal stations had small SSHA (0.49 ± 10.42 cm) and very large GC (83.47 ± 17.30 cm s^{-1}). Although shelf stations displayed SSHA and GC very similar to divergence stations, they were discriminated based on their bathymetry which was significantly shallower (< 1500 m) than at other stations.

The percentage of stations correctly predicted for each of the categories varied from 63 % to 100 % (Table 2). While the predicted category matched the observed category for all anti-cyclonic stations, inconsistencies were noted for the other four categories. During cruise MC10A (Fig. 5), one divergence station (stn 27) was predicted to be cyclonic, and one cyclonic station (stn 46) was predicted to be divergence. The observed SSHA and GC at stn 27 was closer to the mean SSHA and GC for cyclonic stations, probably due to the southward progression of a large cyclonic eddy toward stn 27 (Fig. 5c). At stn 46, SSHA and GC were more closely related to the mean SSHA and GC for divergence stations. This was likely due to the dissipation of the cyclonic anomaly sampled at stn 46 (Fig. 5d). During cruise MC09B (Fig. 4) one frontal station (stn 41) was predicted to be cyclonic, as a result of the much slower GC (54.92 cm s^{-1}) observed at this station. During cruise MC08A (Fig. 3), despite the bathymetry being shallower than 600 m at one shelf station (stn 1176), it was predicted to be frontal due the fast GC (88.72 cm s^{-1}) observed there. A total of 20 cyclonic stations were predicted to be divergent due to their SSHA and GC being more closely related to the mean SSHA and GC for divergence stations. These stations were all associated with the weak cyclonic anomalies sampled at ~15 °S (Fig. 3a) and at ~18 °S (Fig. 3b,c).

The discrepancies between the observed and predicted classification may also be due to limitations associated with satellite altimetry. The coarse resolution of the altimetry data may result in smaller or weaker features not being fully resolved in the gridded maps (Fu et al. 2010), and underestimations of geostrophic current speed are possible since altimeter ground tracks are not always perpendicular to the direction of flow (Backeberg et al., 2008). Close to the coast, altimetry data may be compromised by land contamination and atmospheric correction errors (Madsen et al., 2007). Despite these discrepancies, the DFA classification was shown to be statistically rigorous, and thus the analysis was accepted as providing the final categorisation of all the stations. This predicted classification was used to group the hydrographic data into the five different categories for comparison of the variability between these groups.

3.2. Hydrographic and phytoplankton variability

Hydrographic differences between mesoscale eddies are more pronounced subsurface due to unique dynamic forces resulting in variations of the thermocline and nitracline within these features (Bakun 2006). Means of temperature and salinity at a depth of 100 m, as well as the mean nitracline depth for each of the categories identified by the DFA are shown in Fig. 7. Overall, for all cruises, there were similarities in the pattern of hydrographic variability across the five categories. Temperatures ranged between 15.18 – 25.62 °C, while salinities covered a range of 35.05 - 35.52 psu, and the nitracline depths varied from 15.62 – 123.99 m. Contrasting patterns were observed for temperature and salinity, with the coolest, most saline water discernable at cyclonic stations, while the warmest, freshest water was found at anti-cyclonic stations. The distinctly different temperatures at cyclonic and anti-cyclonic stations are well illustrated in Fig. 8. Temperatures and salinities at divergence and frontal stations were intermediate between these two extremes, with the water at divergence stations tending to be slightly cooler and more saline than the water at frontal stations. Nitracline depths displayed a pattern similar to the temperature variation across the categories. The shallowest nitraclines were associated with the cold saline water at cyclonic stations, while the deepest nitraclines were related to the warm fresh water at anti-cyclonic stations. Divergence stations exhibited slightly shallower nitraclines than those observed at frontal stations.

The observations in this study indicated that the surface waters displayed temperature and salinity (T-S) characteristics which are typical of Tropical and Subtropical Surface Waters from the Indian Ocean, as discussed by Lutjeharms (2006). DiMarco et al. (2002) and Sætre and Jorge da Silva (1984) have demonstrated that these water masses occupy the upper 300 m of the water column throughout most of the Mozambique Channel, with Tropical Surface Water (TSW) generally overlying the Subtropical Surface Water (STSW). Temperatures and salinities at cyclonic stations were consistent with those that describe the more saline STSW, reflecting the upwelling processes which typically occur in cyclonic eddies. Anti-cyclonic stations exhibited T-S properties similar to the less saline TSW, indicating the downwelling processes associated with anti-cyclonic eddies (Bakun, 2006). Divergence and frontal stations showed T-S qualities reflecting a mixture of these water masses (Fig. 7).

Cruise MC10A appeared to be different from the other three cruises. Mean temperature at 100 m was lower and nitracline depths were shallower at frontal stations, while the salinity at divergence stations was lower (Fig. 7). Several frontal stations for cruise MC10A were located close to the

coast at 15 °S (Fig. 5). The interaction of the frontal zone of a cyclonic eddy with the continental slope resulted in the upwelling of cooler water, as illustrated in Fig. 8d, lowering the temperatures at those frontal stations. Divergence stations exhibited lower salinity, most likely due to their location further offshore in areas influenced by anti-cyclonic circulation and downwelling conditions.

At shelf stations, the temperature, salinity and nitracline depths showed considerable differences between cruises (Fig. 7). During cruise MC07, hydrographic characteristics of shelf stations were similar to those observed at anti-cyclonic stations, while they more closely matched the cyclonic stations during cruise MC08A. For cruise MC09B, conditions at shelf stations were comparable to those observed at divergence stations, while during cruise MC10A, they were most similar to frontal stations. Fig. 8 illustrates the likely reasons for the differences observed at shelf stations between the four cruises. During cruise MC07, an anti-cyclonic eddy was located close to the Mozambican coastline causing downwelling along the continental slope, influencing the water mass properties of the shelf stations located there. The orientation of the anti-cyclone along the African coast during cruise MC08A resulted in an intensification of the currents along the shelf edge and the upwelling of cooler water between 15-16 °S. Upwelling of cooler, nutrient rich water in this vicinity has previously been ascribed to the passage of anti-cyclonic eddies (Lutjeharms, 2006; Ridderinkhof and de Ruijter, 2003). Southward and offshore advection of this upwelled water in the periphery of the anti-cyclonic eddy is evident in Fig. 8b, and probably accounts for the similarities in mean nutrient concentrations at cyclonic, divergence, frontal and shelf stations (Fig. 7j). Anti-cyclonic eddies have previously been shown to interact with the Mozambican shelf, entraining and transporting coastal water offshore (Tew-Kai and Marsac, 2009; Quartly and Srokosz, 2004). During cruise MC09B, the alignment of the cyclone/anti-cyclone pair along the Mozambican continental slope (Fig. 4) resulted in the divergence of water from the shelf and the subsequent upwelling of cooler water along the coast at approximately 24 °S, as shown in Fig. 8c. Shelf stations for cruise MC10A were all located at 15 °S, where the frontal zone of a cyclonic eddy interacted with the continental slope, leading to increased current speeds (Fig. 5) and the upwelling of cooler water (Fig. 8d).

In tropical and subtropical oligotrophic ocean regions, mesoscale eddies strongly influence the horizontal and vertical distribution of phytoplankton biomass (Benitez-Nelson et al., 2007; Hansen et al., 2010). In this study, chlorophyll *a* concentrations at the surface were low, ranging between 0.01-1.27 mg m^{-3}, showing little variation between categories. However, at the DCM, chla was

considerably greater, varying from 0.22-9.03 mg m^{-3}, and showed some differences between categories. On average, the depth of the DCM (z_{DCM}) varied from 60-70 m at cyclonic and divergence stations to 80-90 m at frontal, anti-cyclonic, and shelf stations. Overall, the estimated euphotic zone depths were only slightly deeper than z_{DCM}, indicating that the DCM was generally located at the base of the euphotic zone. Integrated chla values reflected the contrasts between the surface and DCM, and confirmed that there were no significant differences between categories in the upper 0-20 m or in the lower 151-200 m layers (Fig. 9). Some differences were observed between categories in the 101-150 m layer for cruise MC07, where the mean integrated biomass was lowest for cyclonic and divergence stations and more elevated at frontal, anti-cyclonic and shelf stations. The largest differences were noted for the 21-100 m layer, where integrated chla was lowest at anti-cyclonic stations and greater at cyclonic stations. Biomass levels were intermediate at divergence and frontal stations for MC07, but more elevated for MC08A (Fig. 9). Shelf stations for MC08A exhibited significantly higher concentrations, yielding a mean value of 61.8 mg m^{-2} compared to 21.9 mg m^{-2} for MC07. The horizontal distribution of the integrated chla for the 0-20 m and 21-100 m depth layers suggested that the highest concentrations were found in the frontal regions, with lower concentrations observed in the cores of cyclonic and anti-cyclonic eddies (Fig. 10). The most striking observation was the band of elevated subsurface chla (Fig. 10d) associated with the nutrient-rich upwelled water along the coast (Fig. 8b). Similar observations of elevated phytoplankton biomass in the coastal region off 16 °S have previously been documented (Lutjeharms, 2006).

The surface layers of oligotrophic ocean regions are characterised by low levels of phytoplankton biomass, while subsurface, phytoplankton often accumulate at distinct depths to form a DCM (Cullen, 1982). In the North Sea, Richardson et al. (1998) concluded that the DCM accounted for up to 75 % of the total areal production. Conversely, in the Atlantic Ocean, the DCM made a minor contribution to the total biomass and production since it formed primarily as a result of lower carbon: chlorophyll *a* ratios at depth (Maranon et al., 2000). In the coastal eastern Indian Ocean, Hanson et al. (2007) found that the carbon content of phytoplankton communities at the DCM was up to five times greater than at the surface and that the DCM contributed significantly to the overall water column primary production. Similarly, this study showed that in the Mozambique Channel, phytoplankton populations in the DCM layer between 21-100 m accounted for 50-82 % of the total biomass in the upper 200 m (Fig. 9).

Several studies have demonstrated that mesoscale eddies markedly influence the spatial structuring of phytoplankton biomass and production. Elevated biomass and production have been associated with cyclonic eddies due to the upwelling of colder nutrient-rich water into the euphotic zone in their centres, while anti-cyclonic eddies show lower biomass and production as a result of the downwelling of nutrient poor surface waters (Benitez-Nelson et al., 2007; McGillicuddy et al., 1998; Waite et al., 2007). Although this study revealed some variations in chlorophyll concentration between cyclonic and anti-cyclonic eddies, these differences were not significant (Fig. 9) and this may be related to elevated grazing by more abundant zooplankton communities in cyclonic eddies as opposed to anti-cyclonic eddies (Huggett, 2012). Omta et al. (2009) suggested that phytoplankton biomass in the Mozambique Channel remains relatively constant throughout the year and that the observed summer minima and winter maxima in satellite chlorophyll *a* concentrations were the result of variations in cellular chlorophyll content. The larger chlorophyll concentrations observed in the frontal regions (Fig. 10), may also be due to the divergent surface flow patterns associated with cyclonic eddies which act to export phytoplankton communities toward the edges of these eddies (Bakun, 2006; Moore et al., 2007; Thompson et al., 2007). Some studies have reported elevated phytoplankton biomass related to anti-cyclonic eddies (Rodríguez et al., 2003; Waite et al., 2007), particularly those which interact with shelf regions and entrain highly productive coastal waters into their boundaries (Crawford et al., 2005; Moore et al., 2007). Most studies investigating the variability of phytoplankton biomass in the Mozambique Channel have been conducted using satellite data (Omta et al., 2009; Tew-Kai and Marsac, 2009), which primarily reflected surface patterns. This study has presented more detail of vertical distributions and demonstrated the importance of the subsurface biomass maxima in the frontal and shelf regions as a consequence of the interaction of mesoscale eddies with the continental slope off Mozambique.

Acknowledgements

We thank the officers, crew and fellow researchers for the success of the surveys conducted on board the *FRS Algoa*, *RV Dr. Fridtjof Nansen*, and the *RV Antea*; and the WIOMSA, MESOBIO, ASCLME, and ACEP programmes, as well as the South African National Research Foundation for funding support and administrative and logistical assistance.

References

Backeberg, B.C., Johannessen, J.A., Bertino, L., Reason, C.J.C., 2008. The greater Agulhas Current system: An integrated study of its mesoscale variability. Journal of Operational Oceanography 1 (1), 29-44.

Backeberg, B.C., Reason, C.J.C., 2010. A connection between the South Equatorial Current north of Madagascar and Mozambique Channel Eddies. Geophysical Research Letters 37, L04604, doi:10.1029/2009GLO41950.

Bakun, A., 2006. Fronts and eddies as key structures in the habitat of marine fish larvae: opportunity, adaptive response and competitive advantage. Scientia Marina 70 (S2), 105-122.

Barlow, R., Lamont, T., Morris, T., Sessions, H., van den Berg, M., 2012. Adaptation of phytoplankton communities to mesoscale eddies in the Mozambique Channel. Deep-Sea Research II (this issue).

Benitez-Nelson, C.R., Bidigare, R.R., Dickey, T.D., Landry, M.R., Leonard, C.L., Brown, S.L., Nencioli, F., Rii, Y.M., Maiti, K., Becker, J.W., Bibby, T.S., Black, W., Cai, W.J., Carlson, C.A., Chen, F.Z., Kuwahara, V.S., Mahaffey, C., McAndrew, P.M., Quay, P.D., Rappe, M.S., Selph, K.E., Simmons, M.P., Yang, E.J., 2007. Mesoscale eddies drive increased silica export in the subtropical Pacific Ocean. Science 316, 1017-1021.

Biastoch, A., Krauss, W., 1999. The role of mesoscale eddies in the source regions of the Agulhas Current. Journal of Physical Oceanography 29 (9), 2303-2317.

Bornman, T., O'Reiley, B., Campbell, E., 2012. Phytoplankton ecology of the Mozambique Channel. Deep-Sea Research II (this issue).

Chapman, P., DiMarco S.F., Davis, R.E., Coward, A.C., 2003. Flow at intermediate depths round Madagascar based on ALACE float trajectories. Deep-Sea Research II 50 (12-13), 1957-1986.

Chelton, D.B., Schlax, M.G., Samelson, R.M., de Szoeke, R.A., 2007. Global observations of large oceanic eddies. Geophysical Research Letters 34, L15606, doi:10.1029/2007GL030812.

Crawford, W.R., Brickley, P.J., Peterson, T.D., Thomas, A.C., 2005. Biological impact of Haida eddies in the eastern Gulf of Alaska, based on SeaWiFS and satellite altimetry observations. Deep-Sea Research II 52, 975-990.

Cullen, J.J., 1982. The deep chlorophyll maximum: comparing vertical profiles of chlorophyll *a*. Canadian Journal of Fisheries and Aquatic Sciences 39, 791-803.

de Ruijter, W.P.M., Ridderinkhof, H., Lutjeharms, J.R.E., Schouten, M.W., Veth, C., 2002. Observations of the flow in the Mozambique Channel. Geophysical Research Letters 29 (10), 1502-1504.

DiMarco, S.F., Chapman, P., Nowlin, W.D., Hacker, P., Donohue, K., Luther, M., Johnson, G.C., Toole, J., 2002. Volume transport and property distributions of the Mozambique Channel. Deep-Sea Research II 49, 1481-1511.

Falkowski, P.G., Ziemann, D., Kolber, Z., Bienfang, P.K., 1991. Role of eddy pumping in enhancing primary production in the ocean. Nature 353, 55-58.

Fu, L.-L., Chelton, D.B., Le Traon, P.-Y., Morrow, R., 2010. Eddy dynamics from satellite altimetry. Oceanography 23(4), 14-25.

Hansen, C., Kvaleberg, E., Samuelsen, A., 2010. Anticyclonic eddies in the Norwegian Sea; their generation, evolution and impact on primary production. Deep-Sea Research I 57, 1079-1091.

Hanson, C.E., Pesant, S., Waite, A.M., Pattiaratchi, C.B., 2007. Assessing the magnitude and significance of deep chlorophyll maxima of the coastal eastern Indian Ocean. Deep-Sea Research II 54, 884-901.

Huggett, J.A., 2012. Mesoscale distribution and community composition of zooplankton in the Mozambique Channel. Deep-Sea Research II (this issue).

Kirk, J.T.O., 1994. Light and photosynthesis in Aquatic Ecosystems. 2nd Edition. Cambridge University Press, Cambridge.

Lévy, M., Shankar, D., André, J.-M., Shenoi, S.S.C., Durand, F., de Boyer Montégut, C., 2007. Basin-wide seasonal evolution of the Indian Ocean's phytoplankton blooms. Journal of Geophysical Research 112, C12014, doi:10.1029/2007JC004090.

Lutjeharms, J.R.E., 2006. The Agulhas Current. Springer, Berlin.

Madsen, K.S., Høyer, J.L., Tscherning, C.C., 2007. Near-coastal satellite altimetry: Sea surface height variability in the North Sea – Baltic Sea area. Geophysical Research Letters 34, L14601, doi:10.1029/2007GLO29965.

Maranon, E., Holligan, P.M., Varela, M., Mourino, B., Bale, A.J., 2000. Basin-scale variability of phytoplankton production and growth in the Atlantic Ocean. Deep-Sea Research I 47, 825-857.

McGarigal, K., Cushman, S., Stafford, S., 2000. Multivariate statistics for wildlife and ecology research. Springer-Verlag, New York.

McGillicuddy, D.J., Robinson, A.R., Siegel, D.A., Jannasch, H.W., Johnson, R., Dickeys, T., McNeil, J., Michaels, A.F., Knap, A.H., 1998. Influence of mesoscale eddies on new production in the Sargasso Sea. Nature 394, 263-266.

Moore, T.S. II, Matear, R.J., Marra, J., Clementson, L., 2007. Phytoplankton variability off the Western Australian Coast: Mesoscale eddies and their role in cross-shelf exchange. Deep-Sea Research II 54, 943-960.

Morel, A., Berthon, J-F., 1989. Surface pigments, algal biomass profiles, and the potential production of the euphotic layer: Relationships reinvestigated in view of remote-sensing applications. Limnology and Oceanography 34 (8), 1545-1562.

Morel, A., Maritorena, S., (2001) Bio-optical properties of oceanic waters: A reappraisal. Journal of Geophysical Research 106 (C4), 7163-7180.

Mostert, S.A., 1983. Procedures used in South Africa for the automatic photometric determination of micronutrients in seawater. South African Journal of Marine Science 1, 189-198.

Omta, A.W., Llido, J., Garçon, V., Kooijman, S.A.L.M., Dijkstra, H.A., 2009. The interpretation of satellite chlorophyll concentrations: The case of the Mozambique Channel. Deep-Sea Research I 56, 974-988.

Oudot, C., Morin, P., Baurand, F., Wafer, M., Le Corre, P., 1998. Northern and southern water masses in the equatorial Atlantic: distribution of nutrients on the WOCE A6 and A7 lines. Deep-Sea Research I 45, 873-902.

Quartly, G., Srokosz, M., 2004. Eddies in the southern Mozambique Channel. Deep-Sea Research II 51, 69-83.

Richardson, K., Nielsen, T.G., Bo Pederson, F., Heilmann, J.P., Lokkegaard, B., Kaas, H., 1998. Spatial heterogeneity in the structure of the planktonic food web in the North Sea. Marine Ecology Progress Series 169, 197-211.

Ridderinkhof, H., de Ruijter, W.P.M., 2003. Moored current observations in the Mozambique Channel. Deep-Sea Research II 50, 1933-1955.

Rodríguez, F., Varela, M., Fernández, E., Zapata, M., 2003. Phytoplankton and pigment distributions in an anticyclonic slope water oceanic eddy (SWODDY) in the southern Bay of Biscay. Marine Biology 143, 995-1011.

Roman, R.E., Lutjeharms, J.R.E., 2007. Red Sea Intermediate Water at the Agulhas Current termination. Deep-Sea Research I 54, 1329-1340.

Roman, R.E., Lutjeharms, J.R.E., 2009. Red Sea Intermediate Water in the source regions of the Agulhas Current. Deep-Sea Research I 56, 939-962.

Sætre, R., da Silva, A.J., 1984. The circulation of the Mozambique Channel. Deep-Sea Research 31 (5), 485-508.

Schouten, M.W., de Ruijter, W.P.M., van Leeuwen, P.J., 2002. Upstream control of Agulhas Ring shedding. Journal of Geophysical Research 107 (C8), 3109-3120.

Schouten, M.W., de Ruijter, W.P.M., van Leeuwen, P.J., Ridderinkhof, H., 2003. Eddies and variability in the Mozambique Channel. Deep-Sea Research II 50, 1987-2003.

Schouten, M.W., de Ruijter, W.P.M., Ridderinkhof, H., 2005. A seasonal intrusion of subtropical water in the Mozambique Channel. Geophysical Research Letters 32, L18601.

Swart, N.C., Lutjeharms, J.R.E., Ridderinkhof, H., de Ruijter, W.P.M., 2010. Observed characteristics of Mozambique Channel eddies. Journal of Geophysical Research 115, C09006, doi:10.1029/2009JC005875.

Ternon, J-F., Barlow, R., Huggett, J., Kaehler, S., Marsac, F., Menard, F., Potier, M., Roberts, M., 2012. An overview of recent field experiments on the ecosystem's mesoscale signature in the Mozambique Channel: from physics to upper trophic levels. Deep-Sea Research II (this issue).

Tew Kai, E., Marsac, F., 2009. Patterns of variability of sea surface chlorophyll in the Mozambique Channel: A quantitative approach. Journal of Marine Systems 77, 77-88.

Tew Kai, E., Marsac, F., 2010. Influence of mesoscale eddies on spatial structuring of top predators'c communities in the Mozambique Channel. Progress in Oceanography 86, 214-223.

Thompson, P.A., Pesant, S., Waite, A.M., 2007. Contrasting the vertical differences in the phytoplankton biology of a dipole pair of eddies in the south-eastern Indian Ocean. Deep-Sea Research II 54, 1003-1028.

van Leeuwen, P.J., de Ruijter, W.P.M., Lutjeharms, J.R.E., 2000. Natal Pulses and the formation of Agulhas Rings. Journal of Geophysical Research 105, 6425-6436.

Waite, A.M., Pesant, S., Griffin, D.A., Thompson, P.A., Holl, C.M., 2007. Oceanography, primary production and dissolved inorganic nitrogen uptake in two Leeuwin Current eddies. Deep-Sea Research II 54, 981-1002.

Weimerskirch, H., Le Corre, M., Jaquemet, S., Potier, M., Marsac, F., 2004. Foraging strategy of a top predator in tropical waters: Great frigatebirds in the Mozambique Channel. Marine Ecology Progress Series 275, 297-308.

Welschmeyer, N., 1994. Fluorometric analysis of chlorophyll *a* in the presence of chlorophyll *b* and phaeopigments. Limnology and Oceanography 39, 1985-1992.

Table 1. Results of the DFA showing the independent contributions of each variable to the three discriminant functions and their related statistics (Wilks' Lambda, Wilks' partial Lambda, F, and tolerance).

	Standardised Coefficients for Canonical Variables			**Discriminant Function Analysis**				
Variable	**DF1**	**DF2**	**DF3**	**Wilks' Lambda**	**Partial Lambda**	**F-remove (4.27)**	**P**	**Tolerance**
SSHA (cm)	0.997	0.166	0.286	0.115	0.235	21.988	<0.001	0.906
GC (cm s^{-1})	-0.302	0.953	-0.214	0.100	0.272	18.081	<0.001	0.957
Bathymetry (m)	-0.024	0.080	1.037	0.058	0.471	7.590	<0.001	0.925

Table 2. Number of correct posterior classifications of station categories (Cyclonic – **C**, Divergence – **D**, Frontal – **F**, Anti-cyclonic – **A**, and Shelf – **S**)

Observed Classification	**Predicted Classification**					**% correctly classified**
	C	**D**	**F**	**A**	**S**	
C	36	21	0	0	0	63
D	1	71	0	0	0	99
F	1	0	59	0	0	98
A	0	0	0	29	0	100
S	0	0	1	0	22	96

Figure Legends

Fig. 1. Map showing the areas sampled during cruises MC07 (September 2007), MC08A (December 2008), MC09B (November 2009), and MC10A (April/May 2010) in the Mozambique Channel.

Fig. 2. (a) Combined maps of merged Sea-surface height anomalies (SSHA) (cm) and Absolute dynamic topography (ADT) ($cm.s^{-1}$) for 19 September 2007. CTD sampling stations for cruise MC07 are indicated as white dots. Bathymetry contours (500, 1000, 2000m) are indicated as thick solid lines. **(b)** Station classification for cruise MC07 (C – Cyclonic, D – Divergence, F – Frontal, S – Shelf, A – Anti-cyclonic).

Fig. 3. Combined maps of merged Sea-surface height anomalies (SSHA) (cm) and Absolute dynamic topography (ADT) ($cm.s^{-1}$) for **(a)** 26 November 2008, **(b)** 3 December 2008, and **(c)** 10 December 2008. CTD sampling stations for cruise MC08A are indicated as white dots. Bathymetry contours (500, 1000, 2000m) are indicated as thick solid lines. **(d)** Station classification for cruise MC08A (C – Cyclonic, D – Divergence, F – Frontal, S – Shelf, A – Anti-cyclonic).

Fig. 4. Combined maps of merged Sea-surface height anomalies (SSHA) (cm) and Absolute dynamic topography (ADT) ($cm.s^{-1}$) for **(a)** 4 November 2009, **(b)** 11 November 2009, and **(c)** 18 November 2009. CTD sampling stations for cruise MC09B are indicated as white dots. Bathymetry contours (500, 1000, 2000m) are indicated as thick solid lines. **(d)** Station classification for cruise MC09B (C – Cyclonic, D – Divergence, F – Frontal, S – Shelf, A – Anti-cyclonic).

Fig. 5. Combined maps of merged Sea-surface height anomalies (SSHA) (cm) and Absolute dynamic topography (ADT) ($cm.s^{-1}$) for **(a)** 14 April 2010, **(b)** 21 April 2010, **(c)** 28 April 2010, and **(d)** 5 May 2010. CTD sampling stations for cruise MC10A are indicated as white dots. Bathymetry contours (500, 1000, 2000m) are indicated as thick solid lines. **(e)** Station classification for cruise MC10A (C – Cyclonic, D – Divergence, F – Frontal, S – Shelf, A – Anti-cyclonic).

Fig. 6. Group centroids and 95 % confidence interval ellipses of the scores for each of the station categories for **(a)** DF1 vs DF2, and **(b)** DF1 vs DF3.

Fig. 7. Box and whisker plots showing the mean and standard deviation of **(a-d)** Temperature (°C), **(e-h)** Salinity, and **(i-j)** Nitracline depth (m) for each station category during cruises MC07, MC08A, MC09B, and MC10A.

Fig. 8. Maps showing the distribution of Temperature (°C) at 100 m for cruises **(a)** MC07, **(b)** MC08A, **(c)** MC09B, and **(d)** MC10A.

Fig. 9. Box and whisker plots showing the means and standard deviation of integrated chlorophyll *a* concentrations over the four depth ranges (0-20m, 21-100m, 101-150m, 151-200m) for each station category during cruises **(a)** MC07, and **(b)** MC08A.

Fig. 10. Integrated chlorophyll *a* for the **(a)** 0-20m depth range (MC07), **(b)** 21-100m depth range (MC07), **(c)** 0-20m depth range (MC08A), and **(d)** 21-100m depth range (MC08A). Note the difference in scaling for integrated chlorophyll *a* for the two depth ranges.

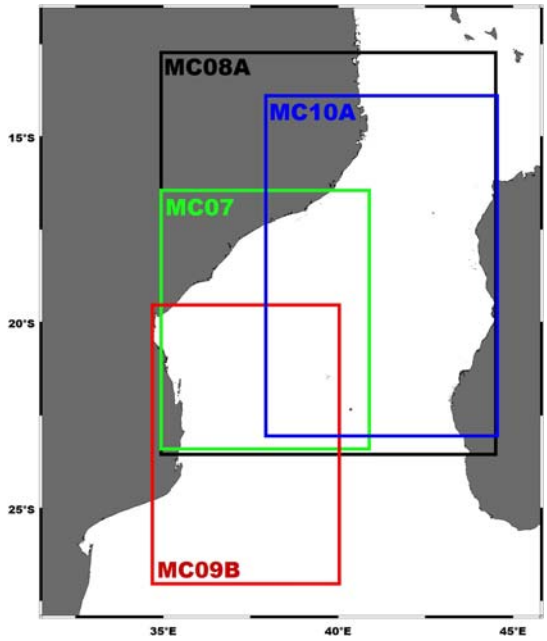

Fig. 1. Map showing the areas sampled during cruises MC07 (September 2007), MC08A (December 2008), MC09B (November 2009), and MC10A (April/May 2010) in the Mozambique Channel.

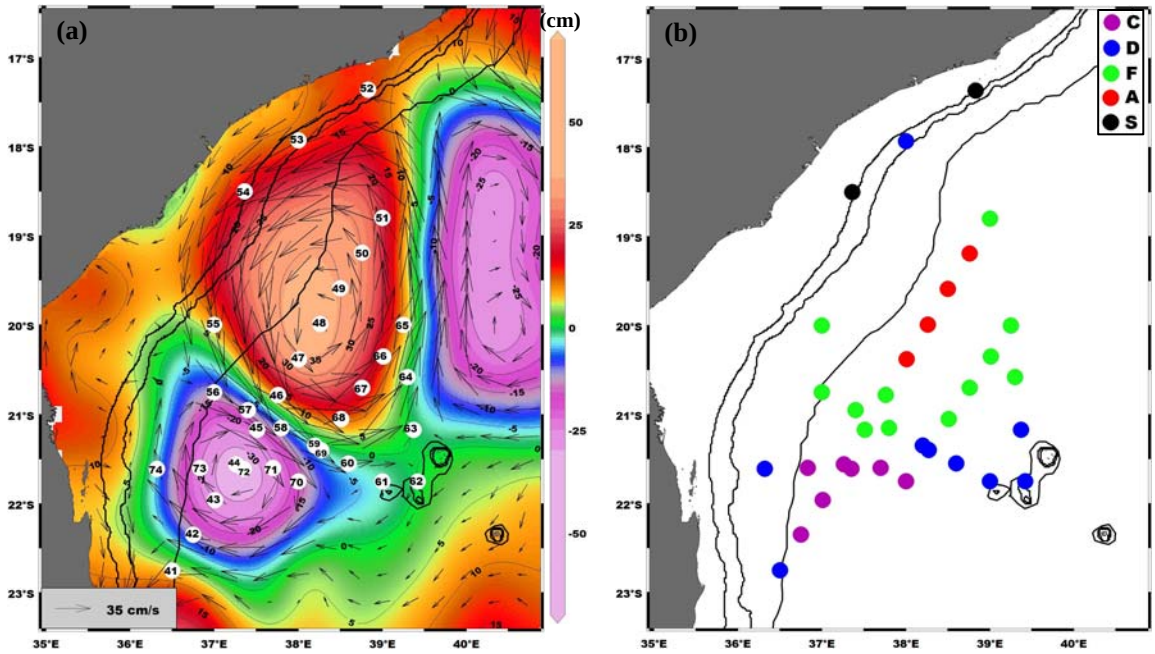

Fig. 2. (a) Combined maps of merged Sea-surface height anomalies (SSHA) (cm) and Absolute dynamic topography (ADT) (cm.s^{-1}) for 19 September 2007. CTD sampling stations for cruise MC07 are indicated as white dots. Bathymetry contours (500, 1000, 2000m) are indicated as thick solid lines. **(b)** Station classification for cruise MC07 (C – Cyclonic, D – Divergence, F – Frontal, S – Shelf, A – Anti-cyclonic).

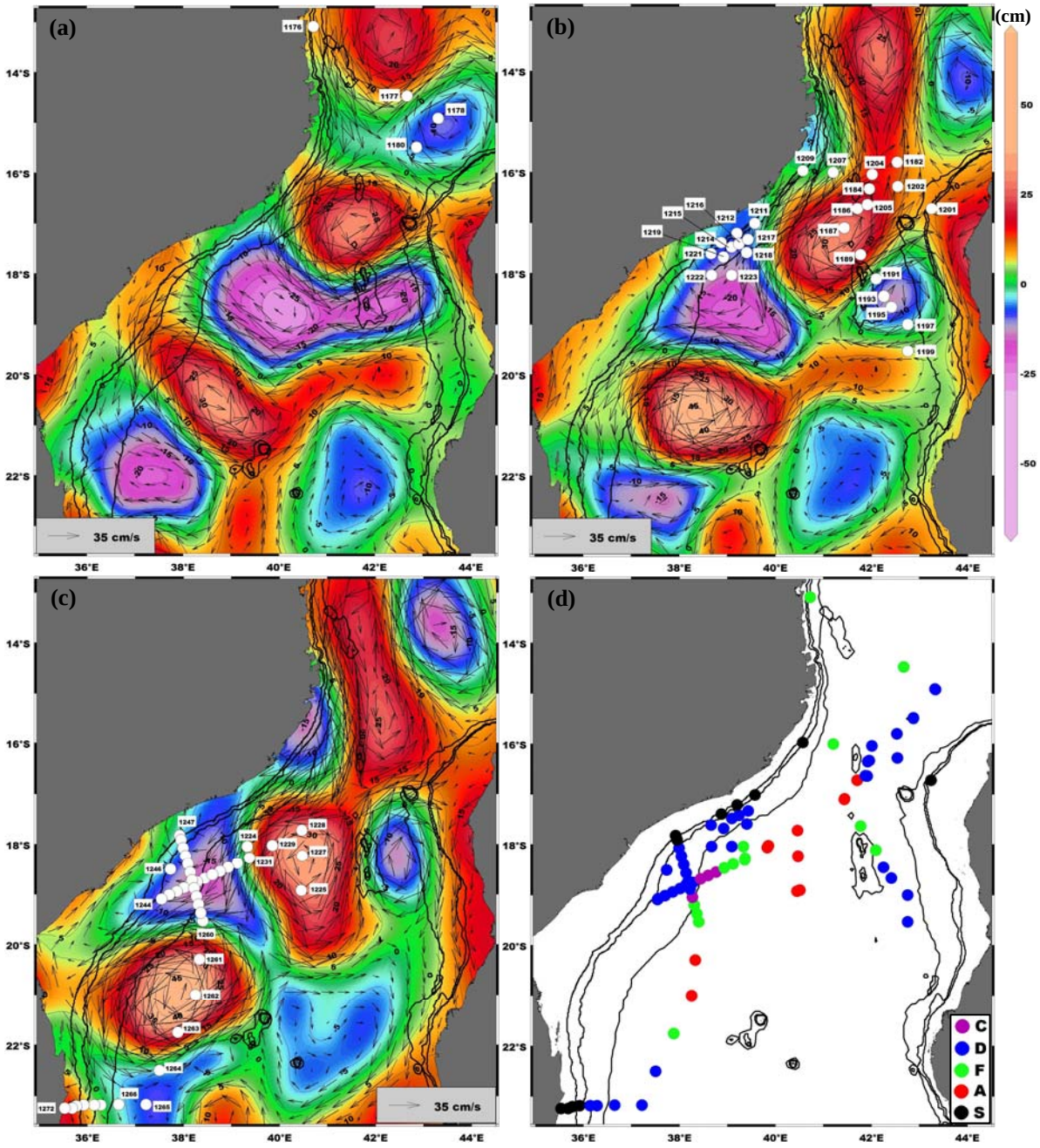

Fig. 3. Combined maps of merged Sea-surface height anomalies (SSHA) (cm) and Absolute dynamic topography (ADT) (cm.s^{-1}) for **(a)** 26 November 2008, **(b)** 3 December 2008, and **(c)** 10 December 2008. CTD sampling stations for cruise MC08A are indicated as white dots. Bathymetry contours (500, 1000, 2000m) are indicated as thick solid lines. **(d)** Station classification for cruise MC08A (C – Cyclonic, D – Divergence, F – Frontal, S – Shelf, A – Anti-cyclonic).

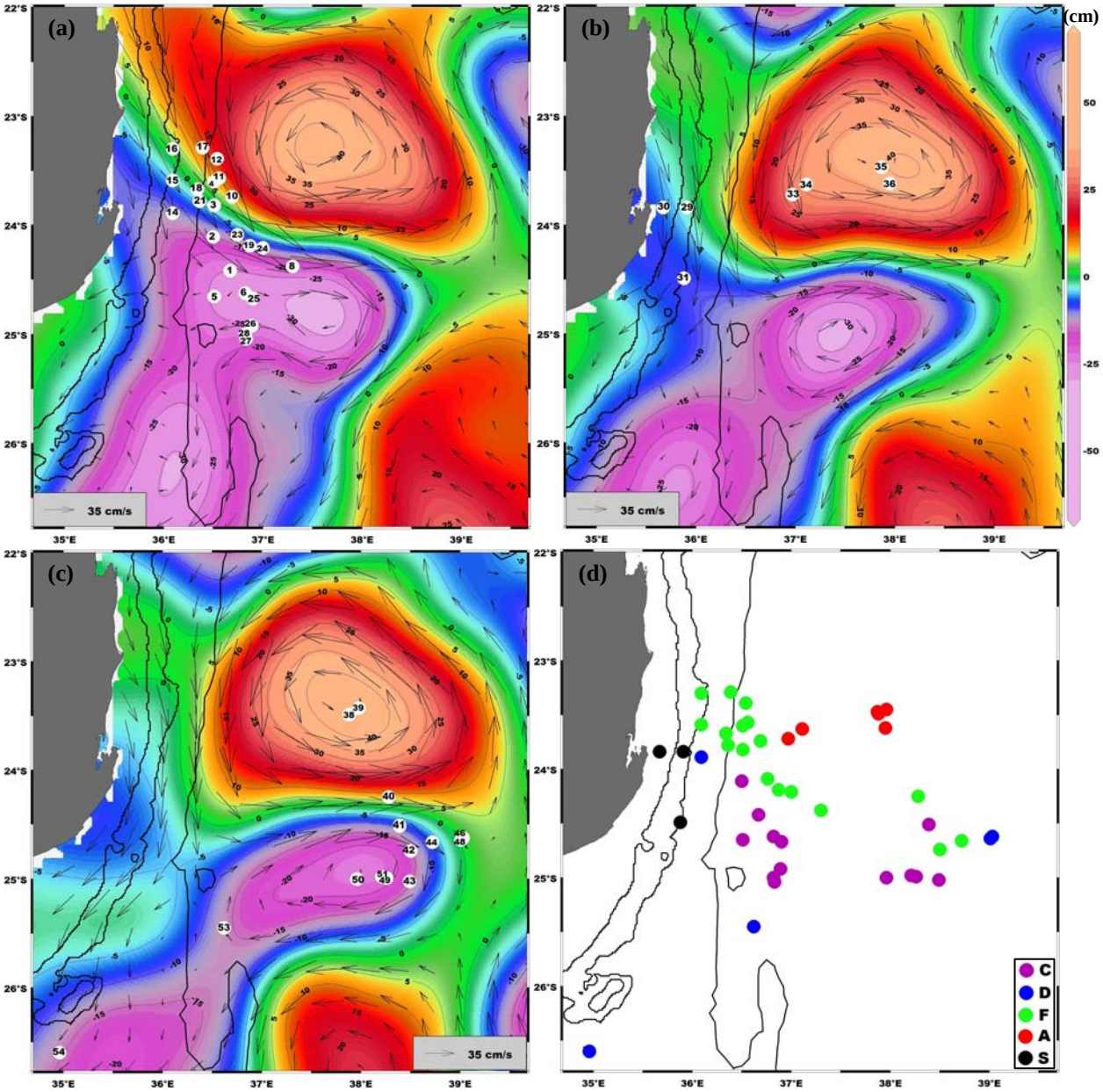

Fig. 4. Combined maps of merged Sea-surface height anomalies (SSHA) (cm) and Absolute dynamic topography (ADT) (cm.s^{-1}) for **(a)** 4 November 2009, **(b)** 11 November 2009, and **(c)** 18 November 2009. CTD sampling stations for cruise MC09B are indicated as white dots. Bathymetry contours (500, 1000, 2000m) are indicated as thick solid lines. **(d)** Station classification for cruise MC09B (C – Cyclonic, D – Divergence, F – Frontal, S – Shelf, A – Anti-cyclonic).

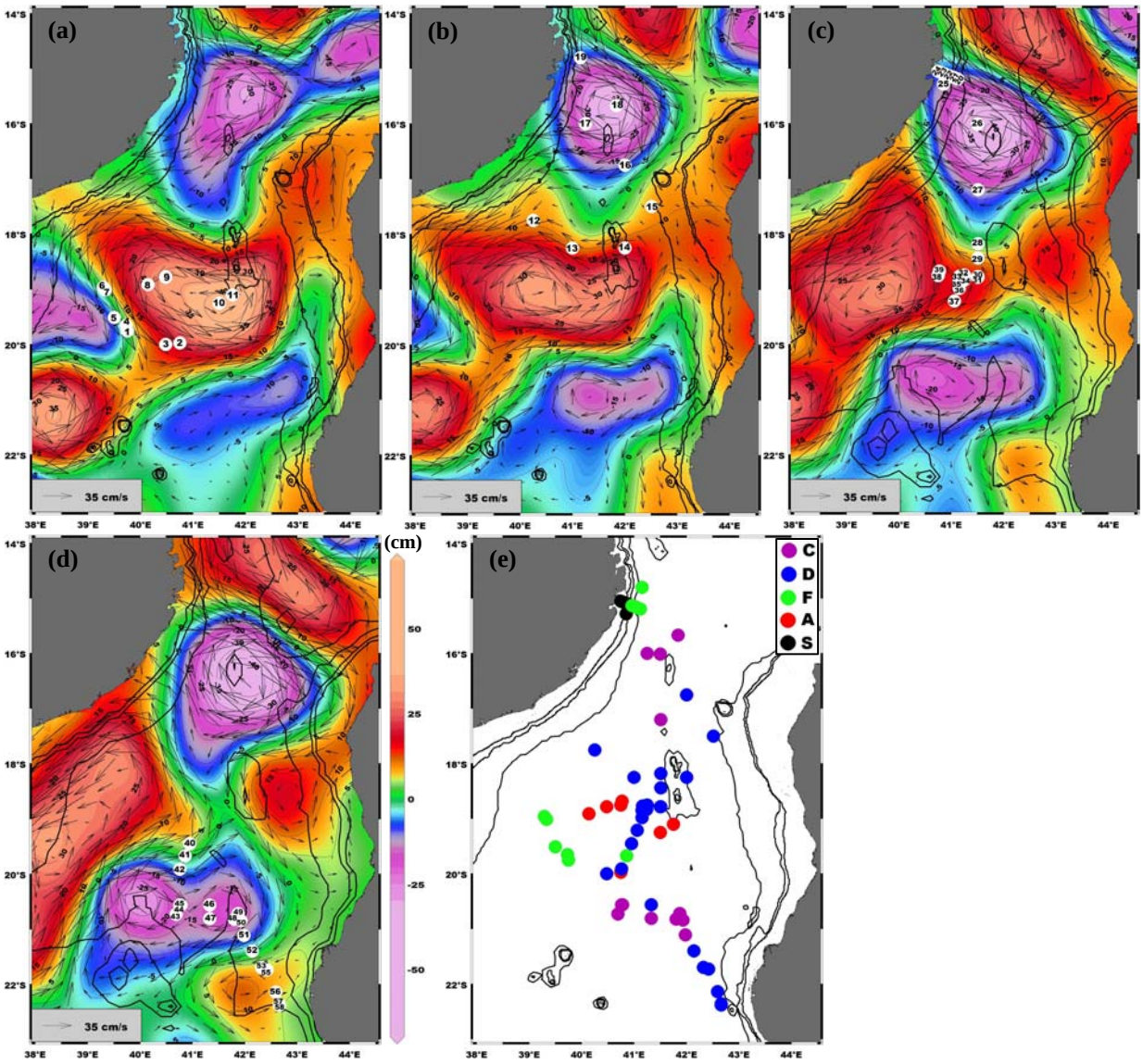

Fig. 5. Combined maps of merged Sea-surface height anomalies (SSHA) (cm) and Absolute dynamic topography (ADT) (cm.s^{-1}) for **(a)** 14 April 2010, **(b)** 21 April 2010, **(c)** 28 April 2010, and **(d)** 5 May 2010. CTD sampling stations for cruise MC10A are indicated as white dots. Bathymetry contours (500, 1000, 2000m) are indicated as thick solid lines. **(e)** Station classification for cruise MC10A (C – Cyclonic, D – Divergence, F – Frontal, S – Shelf, A – Anti-cyclonic).

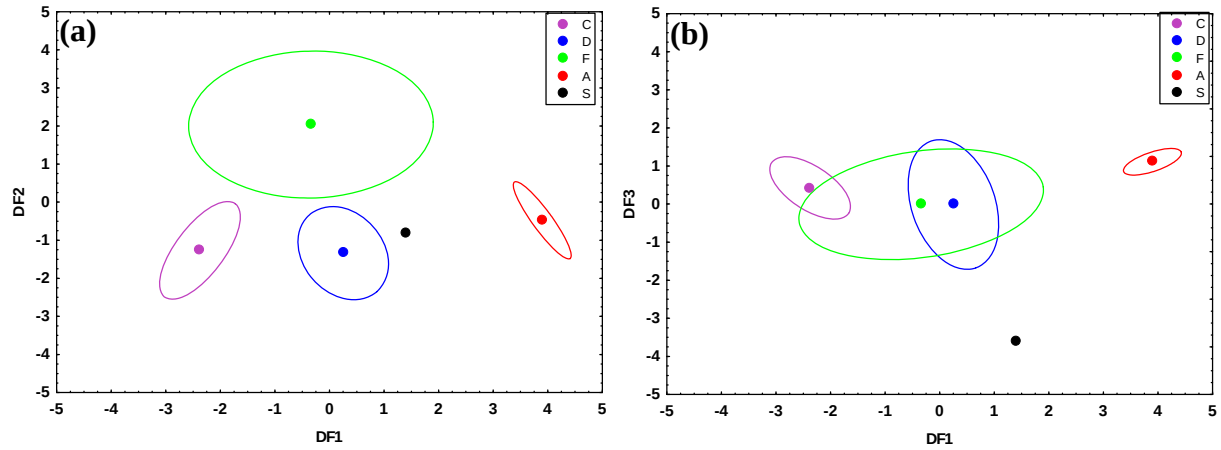

Fig. 6. Group centroids and 95 % confidence interval ellipses of the scores for each of the station categories for **(a)** DF1 vs DF2, and **(b)** DF1 vs DF3.

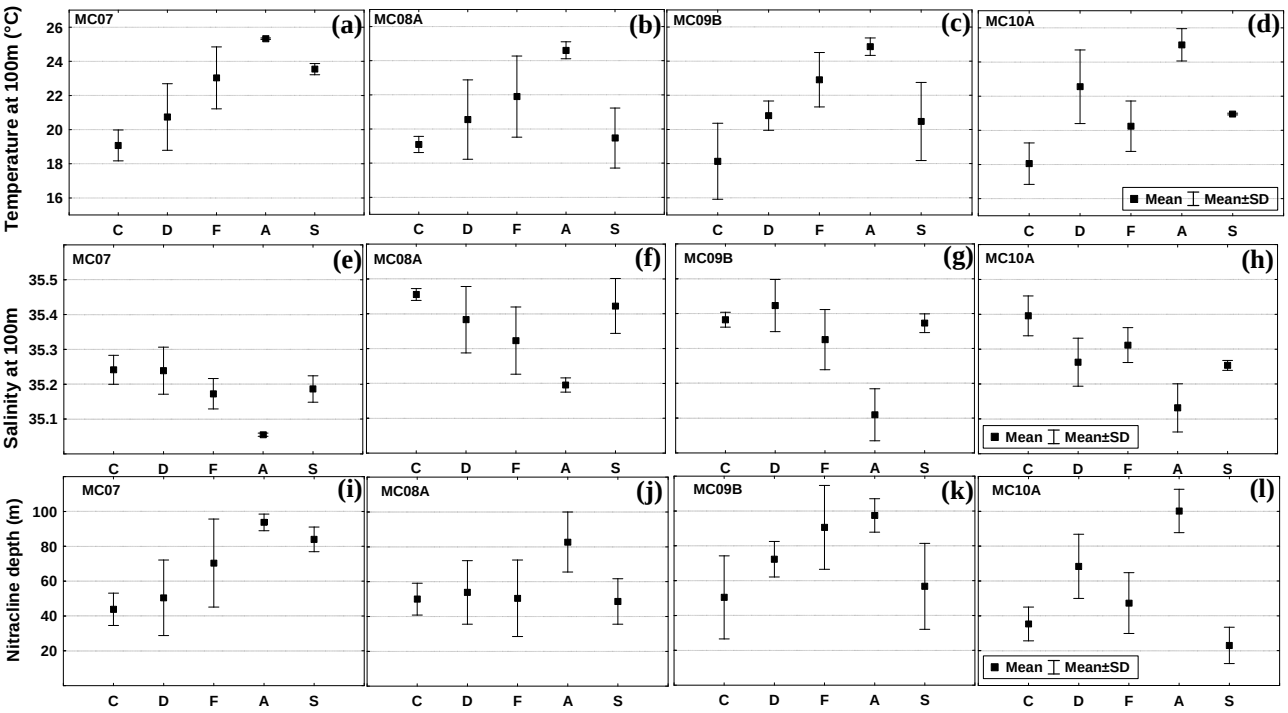

Fig. 7. Box and whisker plots showing the mean and standard deviation of **(a-d)** Temperature (°C), **(e-h)** Salinity, and **(i-j)** Nitracline depth (m) for each station category during cruises MC07, MC08A, MC09B, and MC10A.

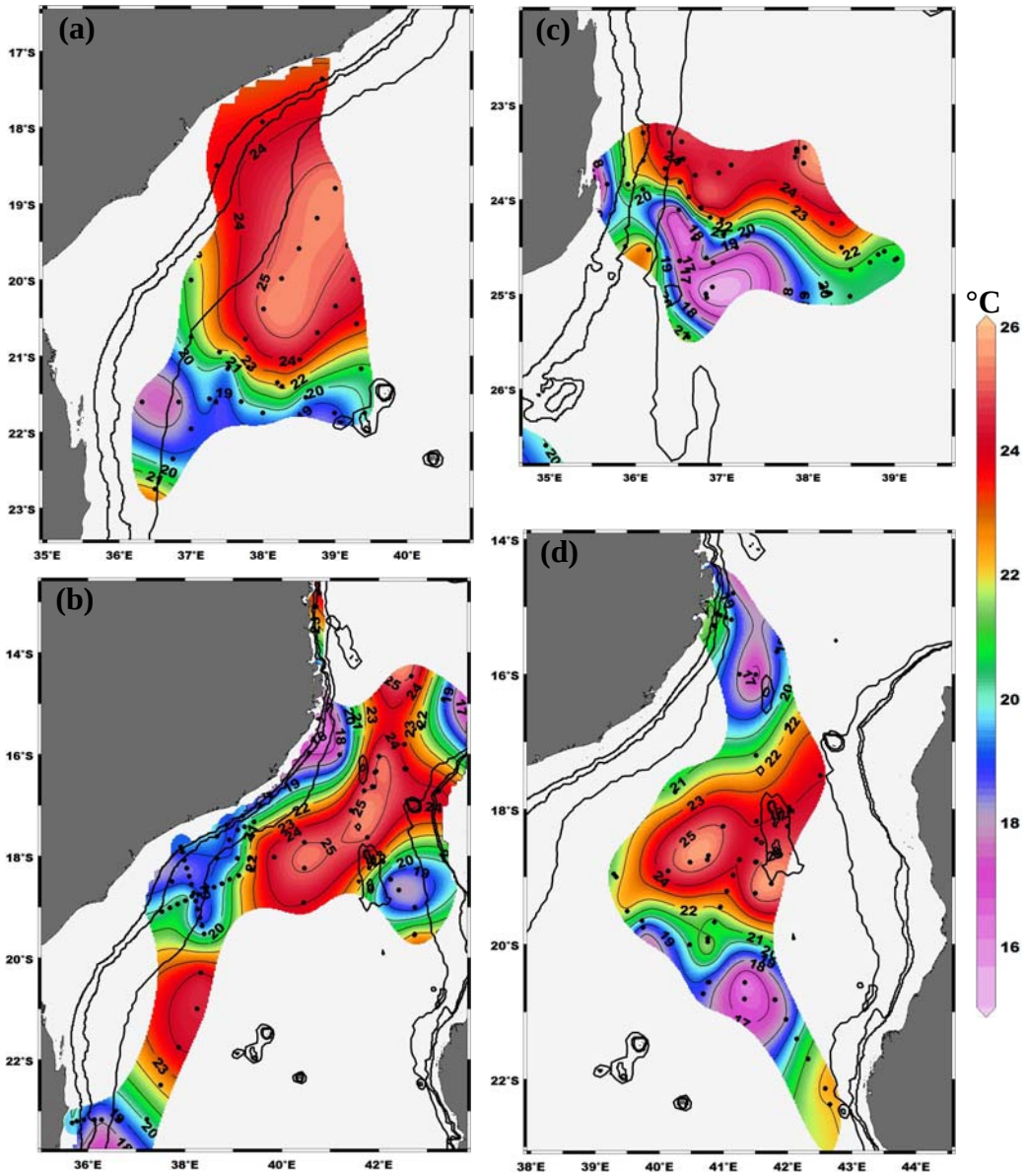

Fig. 8. Maps showing the distribution of Temperature (°C) at 100 m for cruises **(a)** MC07, **(b)** MC08A, **(c)** MC09B, and **(d)** MC10A.

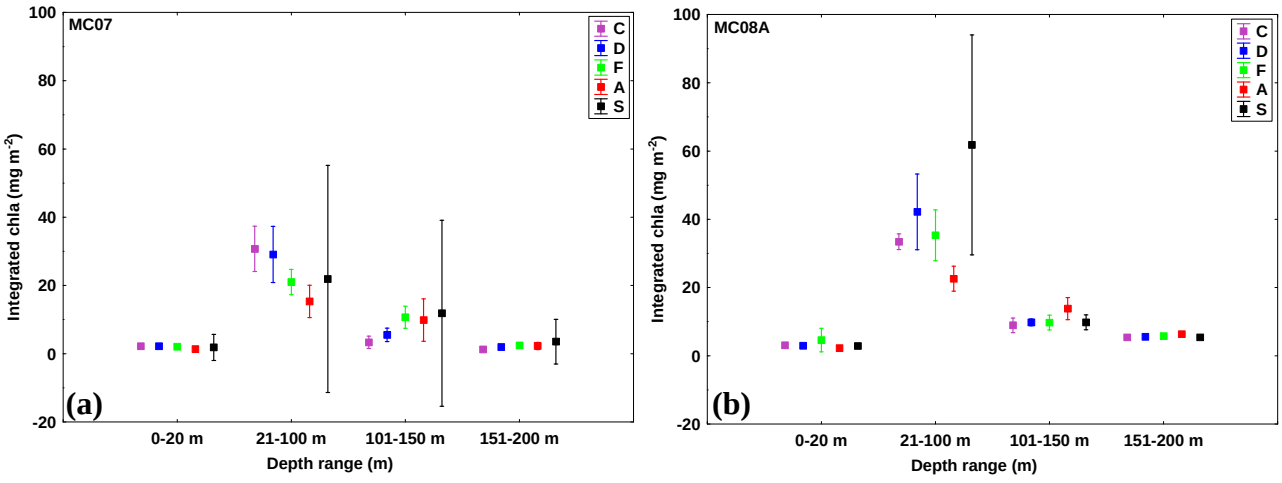

Fig. 9. Box and whisker plots showing the means and standard deviation of integrated chlorophyll *a* concentrations over the four depth ranges (0-20m, 21-100m, 101-150m, 151-200m) for each station category during cruises **(a)** MC07, and **(b)** MC08A.

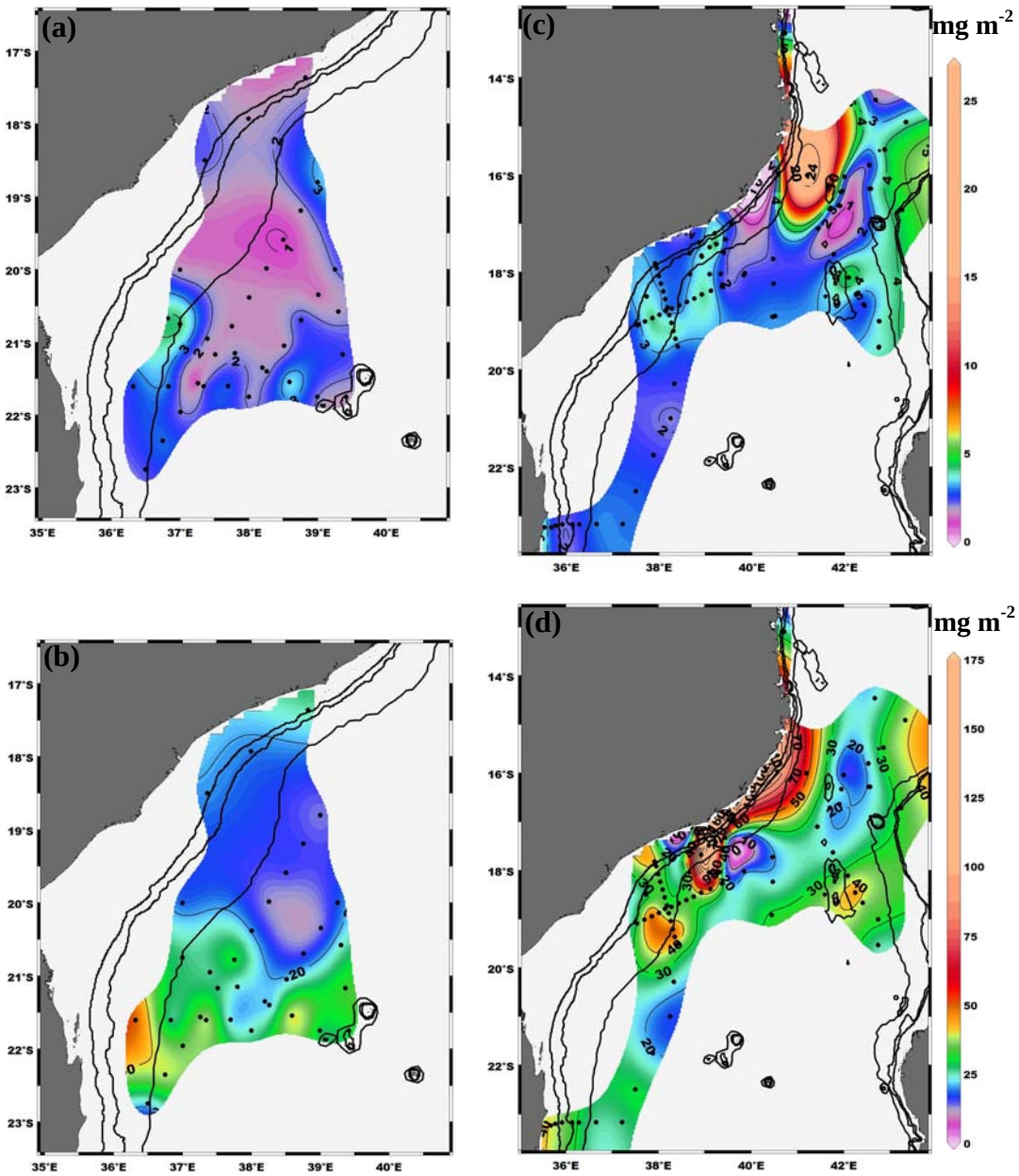

Fig. 10. Integrated chlorophyll *a* for the **(a)** 0-20m depth range (MC07), **(b)** 21-100m depth range (MC07), **(c)** 0-20m depth range (MC08A), and **(d)** 21-100m depth range (MC08A). Note the difference in scaling for integrated chlorophyll *a* for the two depth ranges.